KERNFORSCHUNGSZENTRUM

KARLSRUHE

Juli 1968

KFK 778

Institut für Angewandte Kernphysik

Recent Progress in High Precision Nuclear Spectrometry with Semiconductor Counters

F. Horsch, O. Meyer, W. Michaelis

GESELLSCHAFT FÜR KERNFORSCHUNG M. B. H.

KARLSRUHE

KERNFORSCHUNGSZENTRUM KARLSRUHE

Juli 1968 KFK 778

Institut für Angewandte Kernphysik

Recent Progress in High Precision Nuclear Spectrometry with Semiconductor Counters

by

F. Horsch, O. Meyer, and W. Michaelis

A paper prepared for the international Symposium on nuclear electronics,

Versailles

10 - 13 September 1968

Gesellschaft für Kernforschung m.b.H., Karlsruhe

Recent Progress in High Precision Nuclear Spectrometry with Semiconductor Counters

F. Horsch, O. Meyer, and W. Michaelis

Institut für Angewandte Kernphysik
Kernforschungszentrum Karlsruhe, Karlsruhe, Germany

Abstract:

The paper summarizes the recent progress which has been achieved at Karlsruhe in obtaining optimum precision in nuclear spectrometry with semiconductor counters. One chapter describes new electronic components such as an ultra-high precision pulser for nonlinearity correction, digital stabilization and system checkout, and a timing unit which has been designed for spectrometers where optimum energy resolution is of utmost importance. Another chapter is devoted to ion implantation techniques. The characteristics of ion implanted counters are compared with the performance of detectors produced by diffusion or surface barrier techniques. The dependence of window thickness on reverse voltage, ion energy and ion number and the influence of doping concentration and annealing temperature are discussed. New data are given on the performance of the Karlsruhe Ge(Li) anti-Compton spectrometer. A procedure for computer spectrum analysis is sketched very briefly. To illustrate the high precision which is obtained in radiative neutron capture spectroscopy, results are presented for the first excited states in Zn^{68}.

1. Introduction

In many respects nuclear spectroscopy with semiconductor detectors is now approaching a state which corresponds to the optimum conditions predicted theoretically from the properties of the semiconductor material. Ultra-high precision electronic instruments together with appropriate computer programs for spectrum analysis make feasible accuracies in the energy determination which, some years ago, were believed to be unobtainable. By using advanced spectrometer setups the spectrum shapes can be improved considerably. Both high energy precision and reasonable resolving times are possible in coincidence experiments. New detector fabrication techniques permit the production of devices which show long charge carrier lifetimes and which are more stable to environmental factors than previous devices. The present paper describes the recent progress in high precision nuclear spectrometry achieved in the Karlsruhe research centre.

2. Electronic Components

2.1 Ultra-High Precision Pulse Generator

In order to make full use of the resolution capabilities of semiconductor counters it is necessary to stabilize the gain of the amplifiers and the ADC with digital stabilizers and to correct the channel-energy relationship for nonlinearities of the spectrometer system. For these purposes a pulse generator has been designed [1] which shows very high stability and linearity performance. Using a pulser instead of a natural line for gain stabilization is preferable for two reasons:

1) no background is produced outside the full-energy line and
2) storage of the pulses can be easily prevented by an inhibit circuit.

For the nonlinearity correction a large number of well defined points is required. The accuracy of the pulser should be in the order of 10^{-5} since advanced techniques aim at an accuracy of, for instance, 10 to 100 eV at 2 MeV (see below). The pulse generator described here has an instability of < 10 ppm/°C and a nonlinearity of $\leq \pm 10$ ppm. The most important components of the unit are a Zener diode circuit [2] which is placed in a temperature regulated oven [3] and compensated against variations in temperature and line voltage, a Kelvin Varley precision voltage devider [4] and a chopper stabilized operational amplifier [5] for impedance conversion.

The influence of these components on the performance of the main amplifier output pulse (see Fig. 1) is compiled in Table I. Rising the ambient temperature of the Zener diode to 65 °C by means of a temperature regulated oven lowers its temperature dependence by one order of magnitude. In order to minimize drift each diode was carefully aged for at least 8 weeks under normal conditions. A highly stable 24 V power supply [6] together with the selfstabilizing Zener diode circuit insure the low influence of line voltage variations.

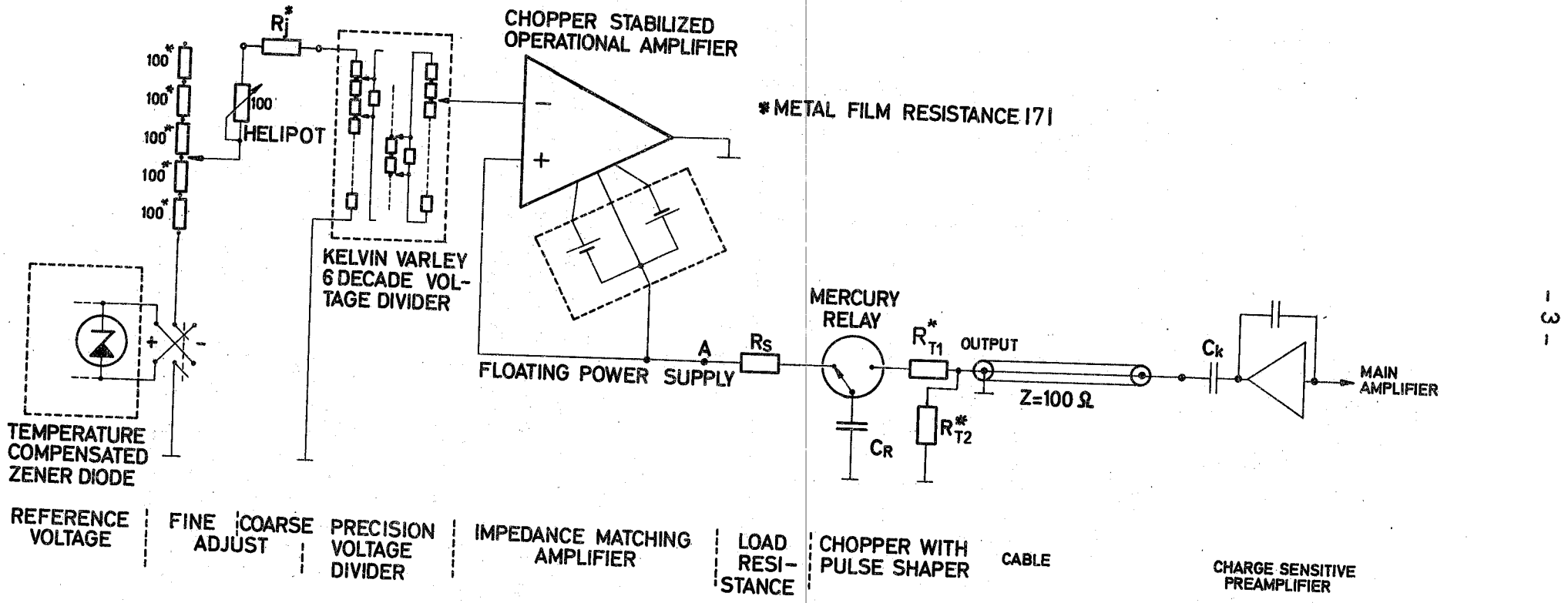

Fig.1 Schematic diagram of the precision pulse generator

Table I

Calculated specifications of the pulse generator components and their influence upon the main amplifier output amplitude

Column No.	1	2	3	4	5	6
Parameter	Reference voltage	Fine and coarse adjust	Voltage divider [b]	Impedance matching amplifier	Pulse shaping capacitor	Mercury relay
Non-linearity			$< \pm 10$ ppm	$\ll 1$ ppm		
Drift per week at constant temperature	$< \pm 1$ ppm [a]	$\leqslant \pm 5$ ppm	$\approx \pm 1$ ppm	$< \pm 10$ ppm dependent on pulse amplitude	$< \pm 10$ ppm	$< \pm 4$ ppm
Temperature dependence	at 25 °C: $< \pm 10$ ppm/°C at 65 °C: ± 1 ppm/°C	± 1 ppm/°C	$\approx \pm 1$ ppm/°C	$< \pm 1$ ppm/°C	$\leqslant 1{,}5$ ppm/°C	$\leqslant 0{,}6$ ppm /°C
Influence of a 1 % line voltage variation	$\ll 1$ ppm			negligible		

[a] measured; [b] manufacturer warranted

Table II

Typical performance characteristics of the precision pulse generator measured at the output of the impedance matching amplifier (point A in Fig. 1)

Parameter	Influence upon output pulse amplitude
Nonlinearity [α]	$\leqslant \pm 10$ ppm
Relative nonlinearity (Fig. 3) of two pulse generator devices	
integral	$< \pm 5$ ppm
differential	$< \pm 25$ ppm
Drift (in 4 weeks at constant temperature)	$\leqslant \pm 5$ ppm
Temperature dependence	+ 3 to + 15 ppm/°C (without temperature regulated oven for Zenerdiode)
Influence of a $\pm$ 20 % line voltage variation	$< \pm 5$ ppm

[α] from Table I

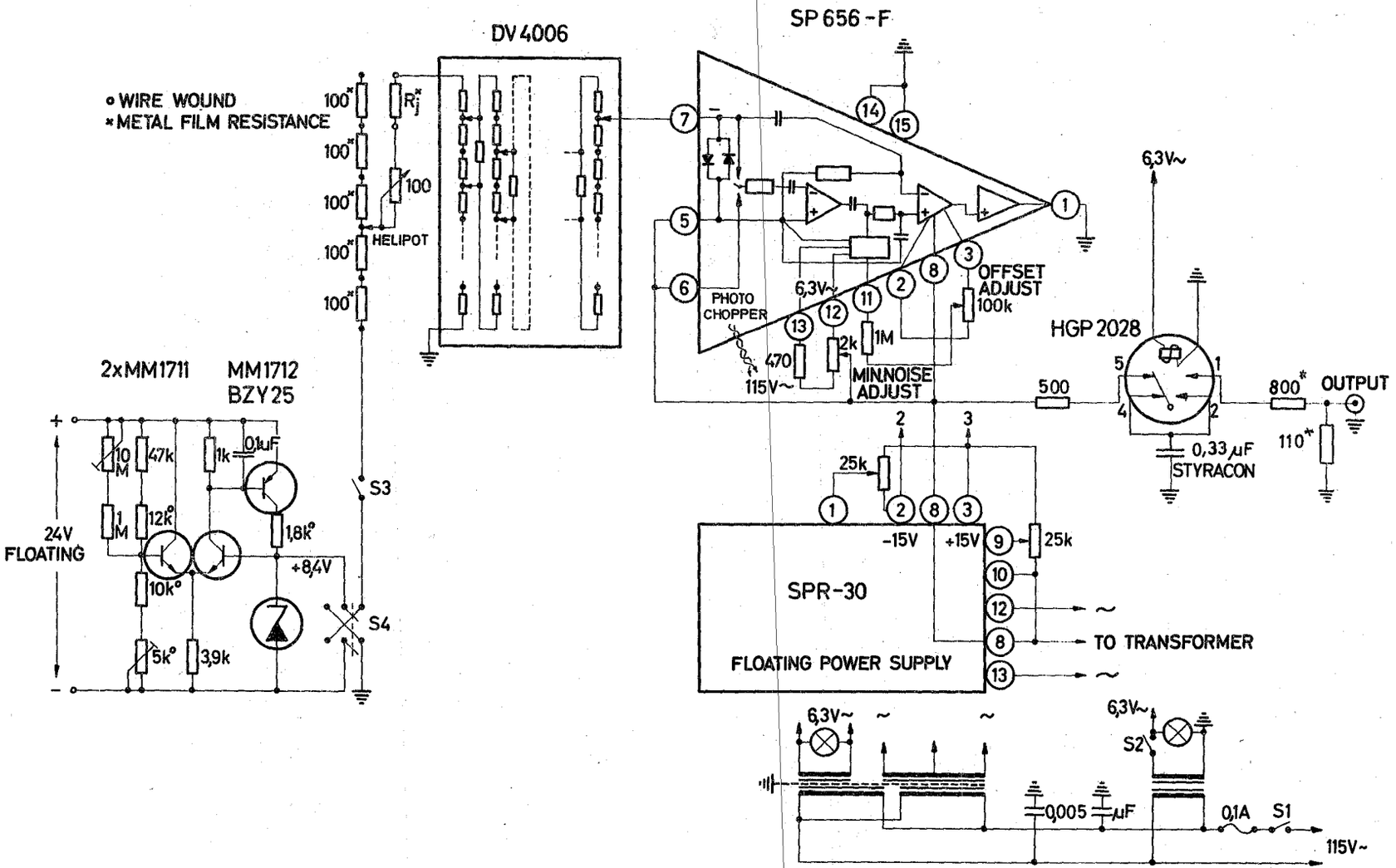

Fig.2 Detailed outline of the precision pulse generator

All resistors labelled with an asterisk (Fig. 1 and 2) are metal film type [7] which have exceeding drift and temperature characteristics. The full linearity of the precision voltage divider can only be realized by using an ultra stable impedance matching amplifier. The chopper stabilized type SP656-F has a manufacturer warranted maximum drift rate of 1 μV per week. Thus for a 10 ppm maximum drift (Table I, Column 4) the dialed voltage at the output of the impedance matching amplifier is limited to $\geqslant$ 100 mV. This gives a 12 mV output pulse if the highest possible amplitude is restricted - by R_{T1} and R_{T2} - to 1 V. If fed into the charge sensitive preamplifier [8] via a 0,6 pF capacitor the specified output pulse amplitude covers an energy range of 120 keV to 10 MeV. The range can easily be modified by means of R_f^*, R_{T1} and R_{T2}.

Instabilities in the pulse shaping capacitor (C_R in Fig. 1) result in a varying decay constant of the output pulse. The influence upon the RC-shaped main amplifier output pulse U is approximately $(dU/U) \approx \frac{T_{max}}{T_R} (dC_R/C_R)$. Here T_{max} is the time where the RC-shaped pulse reaches his maximum ($\approx 3\,\mu$sec for an equal integrating and differentiating time constant of 2 μsec in the main amplifier [9]) and $T_R = (R_{T1} + R_{T2}) \cdot C_R$ the decay constant of the pulse generator output pulse. The best available 0,33 μF capacitors [10] have instabilities in the range of 0,1 % (Column 5) per year. Another instability which may contribute to the overall performance of the precision pulse generator is caused by the $\pm$ 1 mΩ variation [11] of the mercury relay contact resistance which formes a voltage divider with $R_{T1} + R_{T2}$ (Column 6).

Some typical performance characteristics of the unit measured with a digital voltmeter [12] at the output of the impedance matching amplifier are summarized in Table II. The relative nonlinearity (Fig. 3) was determined by measuring the output voltage difference of two pulse generator devices for equal voltage divider settings. A 4 weeks stability test by measuring a 1,019 V output voltage level against a temperature stabilized Weston cell revealed the cited drift value. The same method was applied for determining the temperature dependence. An overall test of the pulse generator by evaluation of computer determined pulser peak positions relative to digitally stabilized natural gamma-ray lines is in progress.

The final version of the precision pulser will have a flip-flop triggered mercury relay and will deliver synchronized gate pulses. In addition, it will be possible to trigger one pulse generator by a second one with a certain time delay for ADC digital stabilization purposes. A variable repetition rate will be provided. At present, 5 pulse generator units are in use for routine nonlinearity correction [13] of experimental setups, digital stabilization and system check-out.

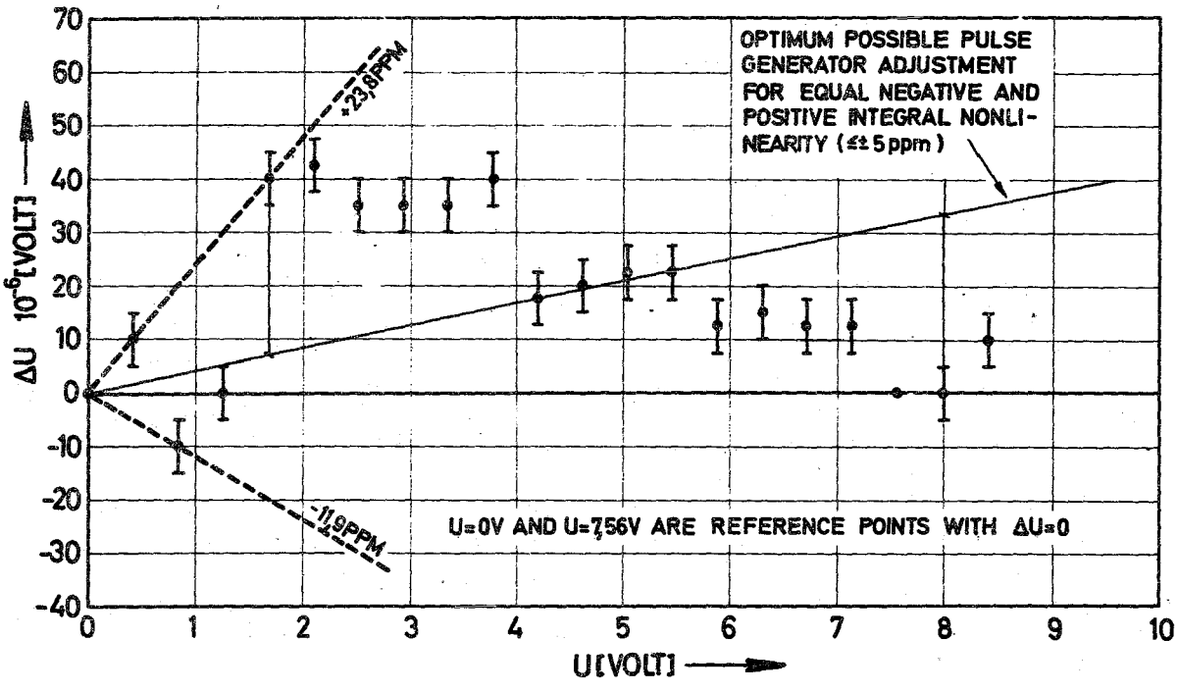

FIG. 3 RELATIVE NONLINEARITY OF TWO PULSE GENERATOR DEVICES

2.2 Timing Unit for Coincidence Experiments

The advances of semiconductor technology have made feasible coincidence experiments involving very high-resolution devices. For applications where optimum energy resolution is of utmost importance a timing unit has been designed which is connected between preamplifier and shaping amplifier [14]. Leading edge timing is used for deriving the time signal. The unit consists of five components: an input fan out circuit, an amplifier stage of medium rise time, a delay-line clipping circuit, a wide-band amplifier and a fast tunnel diode discriminator. The circuit provides reasonable time information even for unfavourable bandwidth performance of the charge-sensitive preamplifier. Employing a liquid scintillator mounted on a 56 AVP photomultiplier and a planar 4.9 cm^3 Ge(Li) detector connected to a preamplifier with 150 nsec rise time the full-width at half-maximum of the time distribution curve was found to be 6.2 nsec if the semiconductor detector was gated on the 1836 keV full-energy peak from an Y^{88} gamma-ray source. The Ge(Li) counter revealed an energy resolution of 2.15 keV FWHM at 662 keV. The timing circuit has been applied succesfully in various coincidence experiments which require utmost precision in the energy determination [13, 15, 16, 17, 18]. No energy resolution degradation has been observed.

3. Ion Implantation Techniques

3.1 Characteristics of Ion Implanted Semiconductor Detectors

Ion implantation techniques are used to produce thin window n^+ and p^+ contacts in silicon, germanium and lithium compensated material. Ion implanted counters show as good performance as detectors produced by diffusion or surface - barrier techniques /19/. Beyond that ion implantation if used under suitable conditions for detector production provides some advantages compared to conventional methods: 1) ion implantation is a low temperature process (annealing temperatures of 150 °C are sufficient) such avoiding thermal degradation of charge carrier lifetime which may occur in the diffusion process, 2) ion doped junctions are more stable to changes of ambient atmosphere and vacuum than surface barrier devices. Systematic studies have been made on the conditions which give optimum detector performance. Interstitial and substitutional doping behaviour of 33 elements have been investigated. A study of the influence of the total number of implanted ions and the target or annealing temperature on the rectifying properties of the diodes has been published elsewhere /20/. New results are summarized in the following subsections.

3.2 Dependence of Window Thickness on Reverse Voltage, Ion Energy, Total Ion Number and Annealing Temperature

The knowledge of the window thickness is most important for the spectroscopy of short range nuclear radiation. Measurements on diffused junction detectors /21/ show the possibility to produce a minimum window thickness of 0.13 μm. For surface - barrier detectors /22/ the window thickness was found to be a function of reverse voltage and doping concentration of the base material, and may range between 0 and 0.2 μm.

In ion implanted counters the window thickness is predominantly a function of ion energy and the angle between ion beam and crystal surface. Beyond that the tail of the depth distribution of electrically active centres in the implanted contact will determine the junction location ($N_A = N_D$). Therefore the window thickness will depend on the doping concentration of the base material, the ion mass and substitution probability, and the annealing behaviour of electrically active defect centres. The window thickness is measured by observing the reduction of alpha particle pulse height as the angle of incidence decreases from 90° /21/. Fig. 4 shows the dependence of the window thickness (B+a) on reverse voltage U_A for boron contacts in n-type silicon, produced with ion energies E of 10, 7, 4 and 2 keV; the total number of boron ions was 10^{13} B^+/cm^2 for each energy. The results may be described by the function (I) $U_A = F\,(B+a)^{-\eta}$. In the case of a step junction and with a depth distribution (II) $N_A(x) = K \cdot x^{-n}$ for the electrically active centres the relation (III) $U_A = \left[q K^2 / 2\varepsilon\varepsilon_o N_D \cdot (1-n)^2\right] \left[(B+b)^{1-n} - (B+a)^{1-n}\right]^2$ is found /23/. (b+B) is the junction location and B = B(E) may be identified with the mean projected range. Comparison of (I) with (III) for high reverse voltage

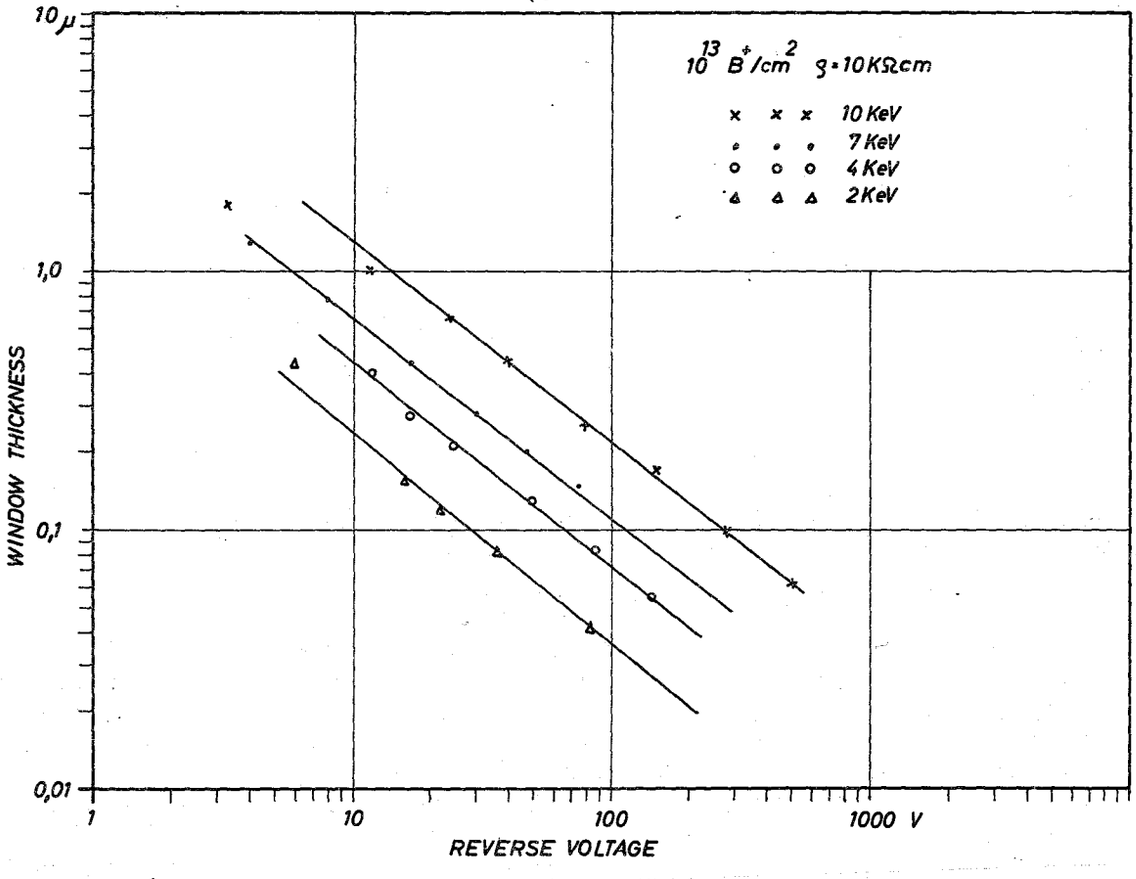

Fig. 4 Dependence of window thickness on reverse voltage and ion energy

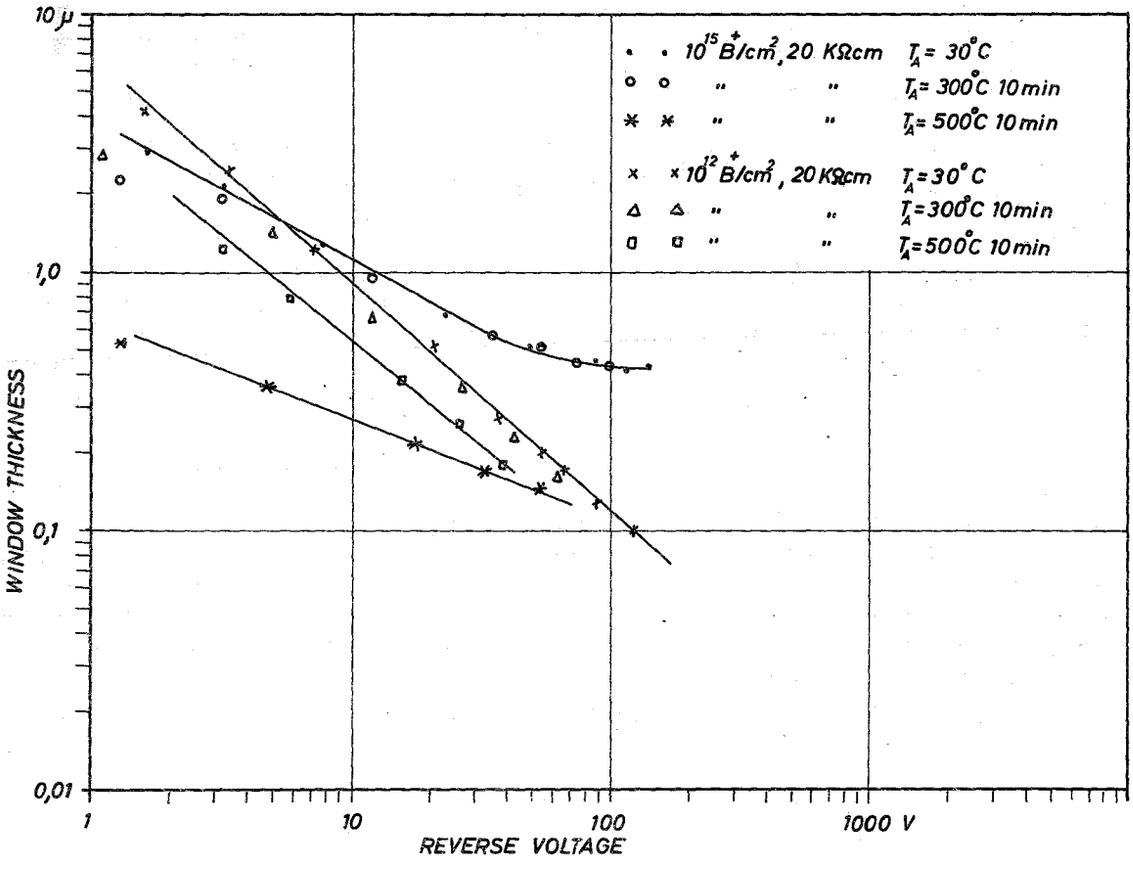

Fig. 5 Influence of the total number of implanted ions and the annealing temperature on window thickness

($b \gg a$) yields $\eta = 2n - 2$ and $K = \left[2 \varepsilon \varepsilon_o N_D (1 - n)^2 F/q\right]^{1/2}$. The analysis of the measurements shows that the exponent η is independent of E ($\eta = 1{,}27$ in Fig. 4) while F is energy dependent. The experiments indicate $F = \text{const } E^{1.25}$. Inserting this into (I) gives $B(E) = \text{const } E^{1.25/1.27}$-a. Thus B(E) turns out to be approximately a linear function of E in this special case of total ion number. This is in agreement with the theoretical result of Lindhard and Scharff /24/.

Fig. 5 shows the results for boron implanted contacts (4 keV) on n-type silicon (20 kΩcm) for total boron numbers of 10^{15} B^+/cm^2 and 10^{12} B^+/cm^2 and for annealing temperatures of 300 °C and 500 °C. The exponent n is dependent on the total implanted ion number: $n = 1{,}57$ for 10^{12} B^+/cm^2 ; $n = 1{,}91$ for 10^{15} B^+/cm^2.

The depth distribution for highly doped contacts shows a strong increase of the exponent n ($n = 3{,}25$) towards the contact surface probably caused by a higher production rate of electrically active defect centres near the surface. Annealing temperatures up to 300 °C have only little influence on the depth distribution; for small voltages, i.e. in the tail of the depth distribution, the concentration of active centres is reduced. Annealing temperatures up to 500 °C lead to a large reduction of concentration. At 500 °C the exponent n for highly doped contacts is found to be 2,3: The annealing effect is larger in the tail of the depth distribution. The same value of 2,3 for the exponent was measured with a capacitance-voltage method by Bower et al. /25/ for the distribution of electrically active centres in antimony contacts (500 °C, 10^{15} Sb^+/cm^2) on p-type silicon.

3.3 Influence of Doping Concentration of the Base Material on Window Thickness

Fig. 6 shows the results for boron implanted contacts (4 keV) on n-type silicon with donor concentrations of $5 \cdot 10^{10}/cm^3$, $2 \cdot 10^{11}/cm^3$ and $6 \cdot 10^{11}/cm^3$. For high resistivity material thin windows require high reverse voltages. The measurements indicate that the depth of active centres is about 500 times larger than the mean projected range for boron ions of that energy (25, 26). F is found to be inversely proportional to N_D; this result is expected from equation (III). By changing the doping concentration of the base material, the depth distribution may be determined over 4 orders of magnitude.

Further measurements on the voltage dependence of the window thickness for implanted contacts, produced with ions of different elements as tellurium, cesium and antimony are shown in Fig. 7. At room temperature the window thickness is about 10 µm for tellurium and cesium contacts and about 3.5 µm for antimony contacts. The window thickness for tellurium contacts decreases continuously for annealing temperatures up to 300 °C. For cesium contacts there is no change for annealing temperatures up to 300 °C. The values for antimony contacts at low reverse voltages are 3,5 µm at 30 °C, 0,4 µm at 300 °C

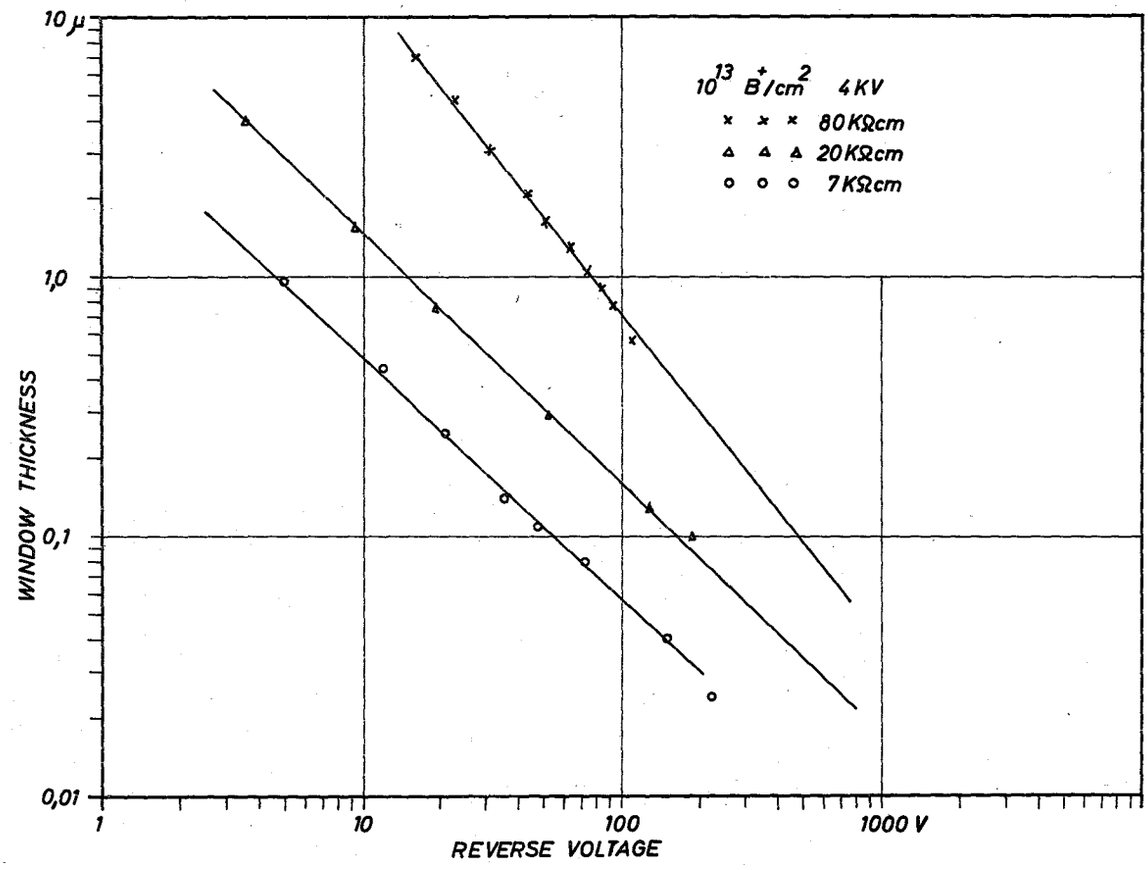

Fig. 6 Dependence of window thickness on the doping concentration of the base material

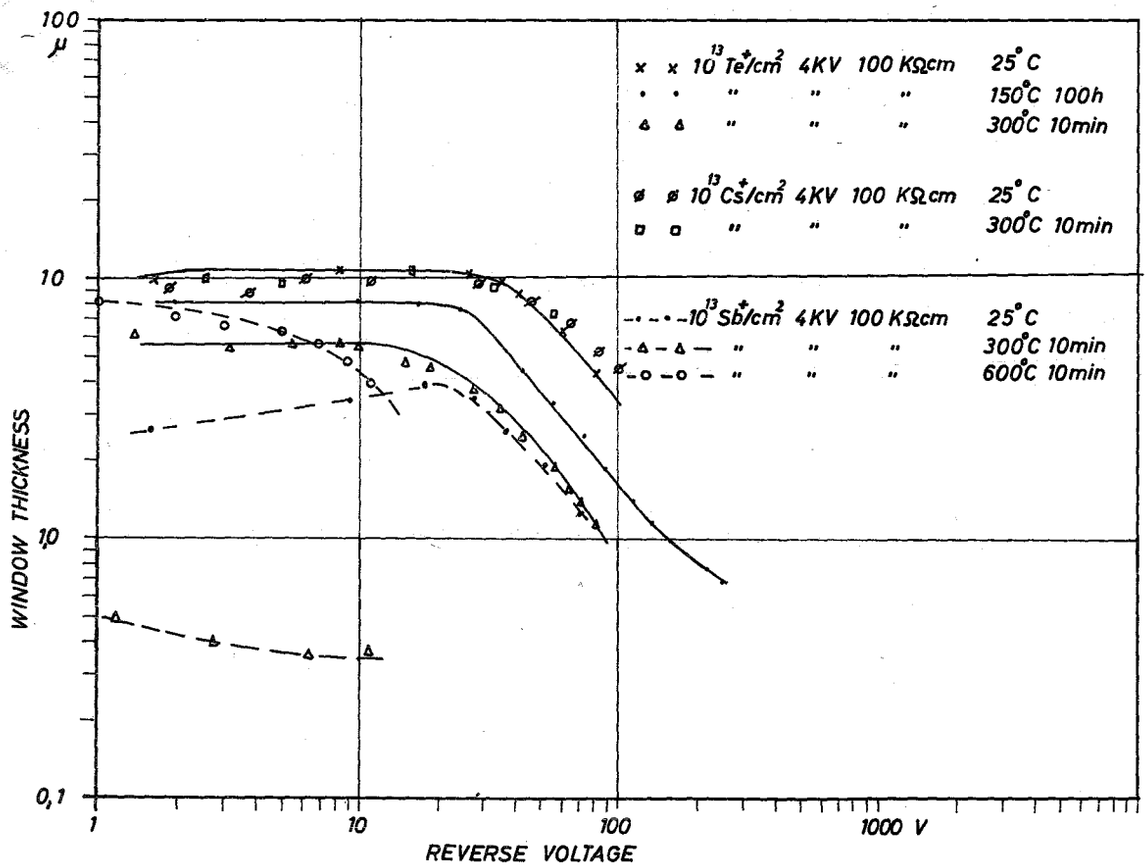

Fig. 7 Window thickness and annealing behaviour for implanted contacts, produced with tellurium, cesium and antimony ions

and 8 μm at 600 °C. The large increase at 600 °C is in agreement with the charge carrier increase measured by Mayer et al. [27]. Further results will be given in a more complete treatment [23].

4. High-Precision Gamma-Ray Spectroscopy Using the Anti-Compton Method

High-resolution measurements of complex gamma-ray spectra in the energy range up to 3 MeV are performed using a Ge(Li) anti-Compton assembly. The spectrometer allows for the special conditions of (n,γ) spectroscopy and gives improved performance compared to previously reported devices. A detailed description was given elsewhere [16]. The setup consists of a 5 cm^3 Ge(Li) diode, a 50 cm dia. x 40 cm plastic scintillator and a 4" dia x 6" NaI(Tl) detector for small scattering angles. The charge-sensitive preamplifier has an input stage with cooled paralleled field-effect transistors [8]. The anti-coincidence method together with a pulse-shape discrimination technique [28] very effectively suppress the Compton background under the peaks. Since our previous paper [16] the performance of the spectrometer has been further improved. The Ge(Li) detector was replaced by another one which is unencapsulated and which shows a more favourable drift geometry (Fig. 8). In this way the amount of absorbing material for the backscattered soft gamma rays is minimized. Furthermore the gain of the preamplifiers connected to the anti-Compton shield detectors has been increased. This allows operating the photomultipliers with improved signal-to-dark current ratios. Fig. 8 illustrates the new performance of the system. The ratio of photopeaks to total height of the background for the Cs^{137} 662 keV gamma ray is 73 : 1 at the Compton edge and about 150 : 1 for smaller scattering angles. Thus the dynamic range of intensities has been further improved. Several hundreds of gamma lines per nucleus are easily detected in the energy range from 100 to 2 000 or 3 000 keV. The energy resolution including long term instabilities is now 1.62 keV FWHM at 662 keV. Correcting this value for leakage current and preamplifier noise yields a statistical width of 1.20 keV and thus a Fano factor of 0.132 which is in good agreement with the result 0.129 ±0,003 reported in ref. [29]. The accuracy which can be obtained in the energy determination is demonstrated in section 5.

5. Spectrum Analysis

For making full use of the anti-Compton spectrometer capabilities detailed analysis of the spectra is performed by means of a computer program. Very promising results have been achieved utilizing the following empirically determined representation of the line shape:

$$y = A \exp\left\{-\lambda (x - x_o)^2\right\} \quad \text{for } x \geq x_o - b \,,$$

$$y = A \left[\exp\left\{-\lambda (x - x_o)^2\right\} - B\, x_{cor} \exp(x_{cor})\right]$$

$$\text{for } x < x_o - b$$

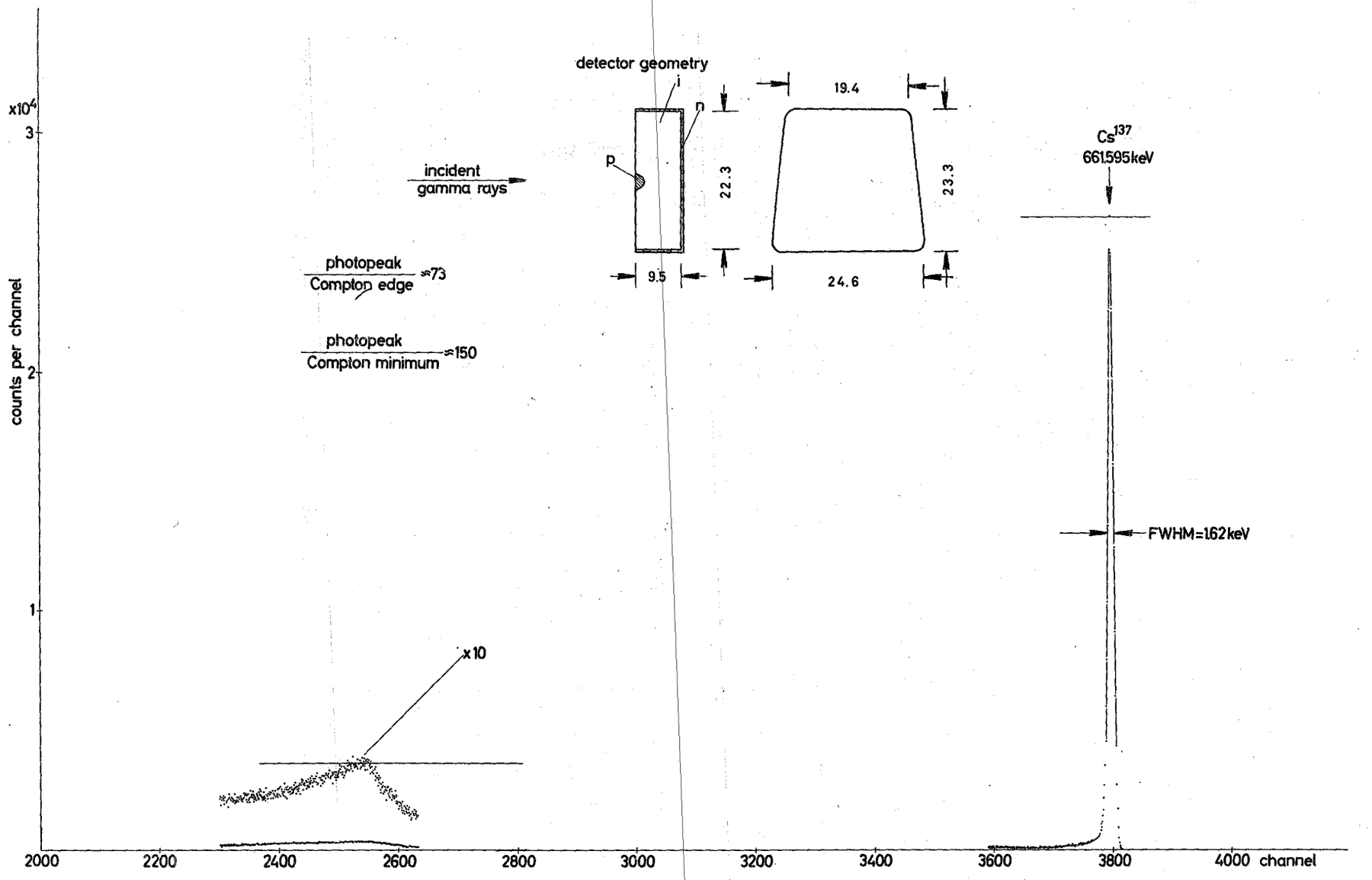

Fig.8 Sectional display of the pulse height spectrum from Cs^{137} taken with the anti-Compton spectrometer

with $b = (\lambda^{-1} \ln 2)^{1/2}$

and $x_{cor} = (x - x_o + b)/b$.

Mathematically these formulae can be handled without difficulty. They are valid for efficient charge carrier collection in the diode. The field strength therefore should be as high as possible. Complex structures are resolved with much success (cf., e.g., /13/). For gamma rays with well-defined spectral peaks accuracies better than 100 eV at 2 MeV have been obtained. This is demonstrated in Table III which gives some results from the neutron capture reaction in Zn^{67}. The absolute errors for the quoted energies are about 50 eV. The errors arising from the fitting procedure and the nonlinearity correction are between 5 and 50 eV. The high accuracy permits the application of Ritz' combination principle to excitation energies in the MeV region. The rapid development will soon ask for an improvement of the data on the absolute energy standards.

Table III

Gamma rays leaving the first excited states in Zn^{68}
(from neutron capture in Zn^{67})

Level	E_{γ_1} /keV/	E_{γ_2} /keV/	E_{γ_3} /keV/	Recoil correction /keV/	Level energy/keV/
1	1077.352	-	-	0.009	1077.361
2	542.345	1077.352	-	0.011	1619.697
3	805.753	1077.352	-	0.014	1883.119
	1883.087	-	-	0.028	1883.115
4	1261.003	1077.352	-	0.022	2338.377
	718.584	542.345	1077.352	0.016	2338.297
9	670.891	Level 4	-	0.004	3009.232
	1126.071	Level 3	-	0.010	3009.198

[1] F. Horsch, KFK 558
[2] INTERMETALL ITT Datenbuch 1967/68 BZY 25
[3] OVENAIRE Type C-113
[4] General Resistance DV 4006
[5] Philbrick Researches Inc., Appl. Manual Section III. 33
[6] LEM Karlsruhe Standard Power Supply
[7] ROSENTHAL Vishay-Rig Type HFE 0809
[8] U. Tamm, KFK 509 (1967)
[9] e.g. ORTEC 410
[10] e.g. SPRAGUE STYRACON, Type 114 P
[11] CLARE Bulletin No. 800 D2
[12] SOLARTRON LM 1420.2
[13] e.g. W. Michaelis, F. Weller, H. Schmidt, G. Markus und U. Fanger: Konfigurationsmischungen in Yb^{169} (submitted for publication in Nuclear Physics)
[14] W. Michaelis, Nuclear Instr. and Meth. 61 (1968) 109
[15] G. Markus, W. Michaelis, H. Schmidt and C. Weitkamp Z. Physik 206 (1967) 84
[16] W. Michaelis and H. Küpfer, Nuclear Instr. and Meth. 56 (1967) 181
[17] W. Michaelis and D. Lange, Nuclear Instr. and Meth. 58(1968)349
[18] F. Horsch, W. Michaelis and H.W. Schmitt, Jülich Conf. 1 (1967) 20
[19] O. Meyer and G. Haushahn, Nuclear Instr. and Meth. 56 (1967) 177
[20] O. Meyer, Proc. of the 11th Scintillation and Semiconductor Detector Symp., Washington, Feb. 1968
[21] R.L. Williams and G.G. Webb, I.R.E. Trans. Nucl. Sci. NS 9, No. 3 (1962) 160
[22] P. Siffert, G. Forcinal and A. Coche I.E.E.E. Trans. Nucl. Sci. NS 14, No 1 (1967) 532
[23] O. Meyer, to be published in Nuclear Instr. and Meth.
[24] J. Lindhard and M. Scharff, Mat. Fys. Medd. Dan. Vid. Selsk. 33, No. 14 (1963)
[25] R.W. Bower et al., Appl. Phys. Letters Vol. 9, No. 5 (1966) 203
[26] J.A. Davies and G. Jespersgard, Can. J. of Physics 44 (1966) 1631
[27] J.W. Mayer et al., Can. J. of Physics 45 (1967) 4073
[28] U. Tamm, W. Michaelis and P. Coussieu, Nuclear Instr. and Meth. 48 (1967) 301
[29] H.R. Bilger, Phys. Rev. 163 (1967) 238